System Level Impact of Landing Point Redesignation for High-Mass Mars Missions

Zarrin K. Chua*, Bradley A. Steinfeldt†, Jenny R. Kelly‡, and Ian G. Clark§

Georgia Institute of Technology, Atlanta, GA 30332-0150

This work presents a preliminary system level assessment of the payload mass change due to landing point redesignation of representative high-mass Mars systems (systems with entry masses greater than 20 t). An optimal propulsive descent guidance law which minimizes the control effort during the descent is used in order to assess the range of feasible landing sites as well as the mass impact on the payload of the system. It is shown that either increasing the entry mass or delaying the time of redesignating the landing site decreases the payload capability of reaching the surface as well as reduces the number of reachable landing sites. In addition, it is shown that the payloads associated with supersonic retropropulsion are more sensitive to the landing point redesignation time than systems using inflatable aerodynamic decelerators.

I. Introduction

MANKIND has continually set its eye on exploring the Red planet. The Martian environment is harsh - not only is there a thin atmosphere with large uncertainties, there are mountains, volcanoes, canyons, craters, rocks, and dust on the surface. Each of these surface hazards complicate the selection of landing sites for exploration missions, causing mission designers to trade the scientific return (interesting landing sites are often in hazardous regions) with mission safety (desirable to be far away from these hazards). The delicate balance between these two objectives is shown in Fig. 1, which depicts the number of rocks per hectare that are greater than 1.5 m in diameter from observations using the High Resolution Imaging Science Experiment (HiRISE) in (a) the Phoenix landing region with potential landing ellipses superimposed and (b) a 25 km $\times$ 25 km subset of the rock count data. There are no landing ellipses for the Phoenix mission in which no significant rock hazards exist. Even if pinpoint landing capability (within 100 m of the intended target[1]) is achievable on Mars, *a priori* imaging capability from orbital assets is unlikely to give full knowledge regarding the surface terrain in order to guarantee a safe landing. This lack of certainty is a particularly daunting thought when considering the prospect of selecting a safe landing site for high-mass mission (possibly with humans onboard). One way to increase the probability of a safe landing is to give the system the capability to perform a propulsive divert maneuver once a hazard is identified. This approach was implemented during the Apollo lunar campaign and investigated in depth by the Autonomous Landing and Hazard Avoidance Technology (ALHAT) project and elsewhere.[2–4]

The objective of this investigation is to provide a quantitative assessment at the system level of the impact of such divert maneuvers for high-mass Mars missions (either robotic or crewed). The primary metric used for this examination is the payload mass that the system is capable of delivering to the Martian surface. Additionally, this metric provides insight into the feasibility of landing sites for a required payload mass and delivered accuracy requirement (for a fixed guidance algorithm). The results build upon the work developed by Steinfeldt, *et al.* in which the payload capabilities for various high-mass Mars entry systems were identified.[7] In that study, deterministic results were presented for non-precise, soft landings on the Martian surface. In the current investigation, the system level ramifications of the landing point redesignation (LPR) are assessed by (1) changing the time of the redesignation and (2) changing the designated landing site. Varying these parameters results in a payload mass change that can be assessed deterministically and probabilistically. These sensitivities are explored for a 20 t entry vehicle and a 100 t entry vehicle. In addition to examining the sensitivity with respect to entry mass, the sensitivity is further examined with respect to supersonic

*Graduate Research Assistant, Guggenheim School of Aerospace Engineering, AIAA Student Member, zarrin@gatech.edu

†Graduate Research Assistant, Guggenheim School of Aerospace Engineering, AIAA Student Member, bsteinfeldt@gatech.edu

‡Research Engineer, Guggenheim School of Aerospace Engineering, AIAA Member, jenny.kelly@gatech.edu

§Visiting Professor, Guggenheim School of Aerospace Engineering, AIAA Member, ian.clark@gatech.edu

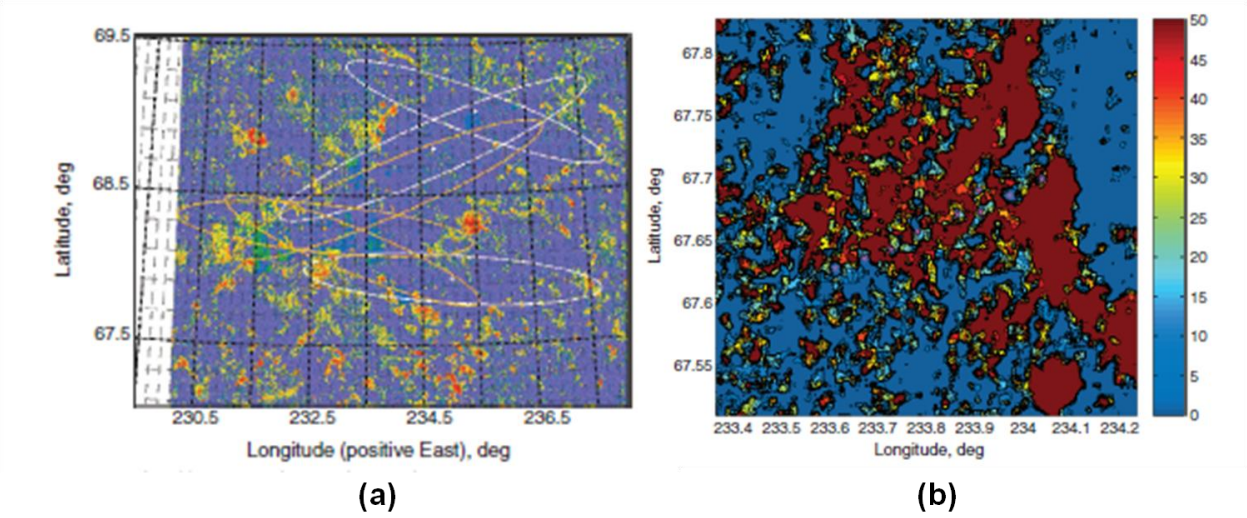

Figure 1: Rock count data for (a) the Phoenix landing site region and (b) a 25 km $\times$ 25 km subset of the data.[5,6]

deceleration technology, where inflatable aerodynamic decelerators (IAD) and supersonic retropropulsion (SRP) are considered.[8,9]

II. Modeling and Simulation

A. Nominal Entry System Sizing

Two representative nominal cases which span the potential entry masses for high-mass Mars missions are under investigation by the community.[7,10–12] These two cases are based upon the results presented in Steinfeldt, *et al*[7] and have entry masses of 20 t and 100 t. Each vehicle nominally delivers 9.2 t and 42.1 t of payload to the surface, respectively, using a supersonic IAD. The aeroshell for both vehicles is a 10 m diameter, 70° sphere-cone aeroshell with a hypersonic lift-to-drag ratio of 0.3 (Fig. 2). The vehicle with a 20 t entry mass uses a 20 m tension cone IAD while the 100 t entry mass system uses a 50 m tension cone. In addition to supersonic IADs, another supersonic deceleration

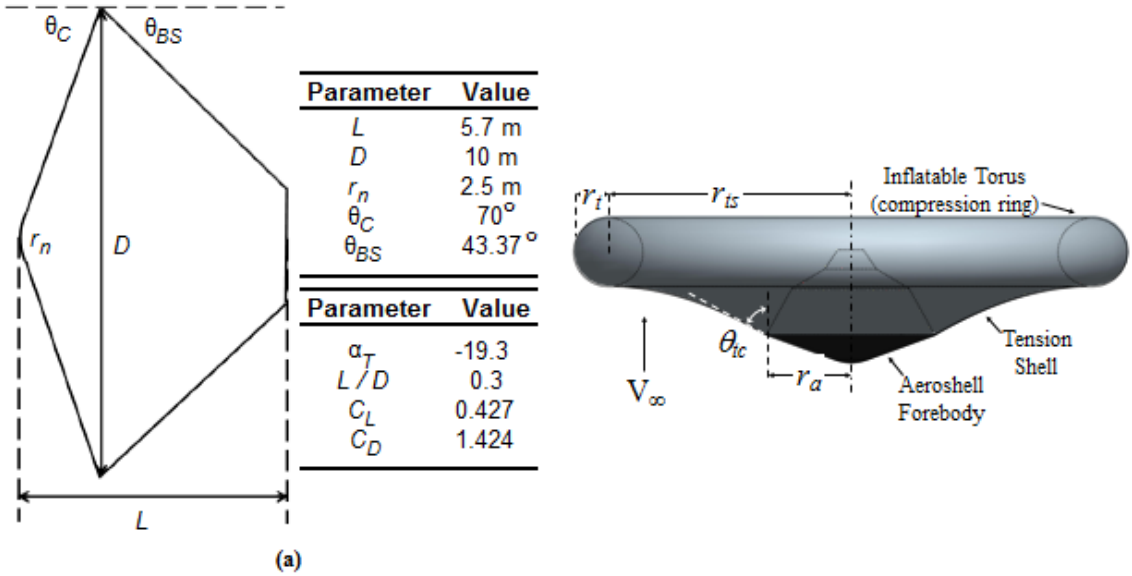

Figure 2: Geometry of (a) the 70° sphere-cone aeroshell and (b) supersonic IAD.[7]

technology, SRP, is examined with a 20 t entry mass vehicle to investigate the sensitivity to supersonic deceleration technology. This 20 t entry vehicle is nominally able to supply 5.3 t of payload to the Martian surface. For all cases, the propulsive descent is achieved through a LOx/CH_4 engine with a specific impulse of 350 s and a maximum thrust-to-vehicle weight ratio of 3.0 (relative to Earth). Table 1 lists a summary of the nominal vehicle trajectory and sizing characteristics for each of the cases considered.

Table 1: Trajectory and Mass Characteristics for the Nominal Cases.

	20 t IAD	**100 t IAD**	**20 t SRP**
Flight Time, s	82	34	57
Maximum Thrust, kN	549	2638	402
Tension cone diameter, m	20	50	N/A
Tension cone C_D	Mach Dependent[7]	Mach Dependent[7]	N/A
Aeroshell C_D	1.424	1.424	1.424
Aeroshell C_L	0.427	0.427	0.427
Hypersonic L/D ratio	0.3	0.3	0.3
Structural Mass, kg	2,115	14,810	1,858
Heatshield Mass, kg	830	6,130	990
Backshell Mass, kg	2,800	14,000	2,800
RCS System Mass, kg	100	500	100
IAD Mass, kg	514	4,250	N/A
SRP Propellant, kg	N/A	N/A	5,354
RCS Propulsion Mass, kg	304	1,520	304
Descent Propellant Mass, kg	2,434	7,502	922
Propulsion System Mass, kg	470	1,206	796
Payload Mass, kg	*9,164*	*42,073*	*5,268*
Payload Mass Fraction, -	0.46	0.42	0.26

B. Initial Conditions

The nominal conditions at propulsive descent initiation (PDI) are identical to those found by Steinfeldt, *et al.*[7] Steinfeldt, *et al.* had determined a set of optimal trajectories that maximize the payload mass for a soft-landing on the Martian surface by controlling the bank angle profile through the hypersonic regime. After deceleration through the hypersonic and supersonic regimes, PDI begins at Mach 0.8. The conditions at PDI used for this study are shown in Table 2 where the difference in entry mass and the mass at PDI is a result of the heatshield and IAD being shed prior to PDI or the consumption of propellant during SRP.

Table 2: Initial Conditions at PDI for the Investigated Cases.

	20 t IAD	**100 t IAD**	**20 t SRP**
Altitude, km	9.82	2.69	5.48
Flight Path Angle, deg	-79.6	-49.7	-56.7
Velocity, m/s	193.3	196.8	194.0
Mass at PDI, t	18.4	89.6	13.7

C. Trajectory Propagation

The 3-DOF propulsive descent trajectory uses a general optimal planetary landing guidance law. The general optimal planetary landing guidance law developed by D'Souza is a closed-loop, analytic guidance law that minimizes the linear combination of the flight time and the control effort (*i.e.*, the acceleration) expended during the descent.[13] A

weighting on the time-to-go was chosen in this implementation of the guidance algorithm to prevent subterranean trajectories. In this algorithm, there is not an explicit constraint for the maximum thrust. However, in this study's implementation, should the thrust exceed the maximum allowable thrust of the vehicle, the vehicle is commanded to apply the maximum thrust along the commanded direction. The nominal landing sites were chosen to be consistent with Steinfeldt, *et al.* where the terminal descent trajectory is governed by a gravity turn.[7] These are near propellant optimal landing sites and represent the maximum payload cases for each of the nominal trajectories. Trajectories were propagated using two methods: a variable-step fourth-order Runge-Kutta algorithm with fifth-order truncation was used for the deterministic analysis, and a fourth-order Runge-Kutta scheme with a fixed 0.5 s timestep was used for the probabilistic analysis. The trajectory propagation terminates when the altitude is less than 10 m. The nominal propulsive descent trajectory for each of the entry mass and decelerator combinations analyzed is shown in Fig. 3.

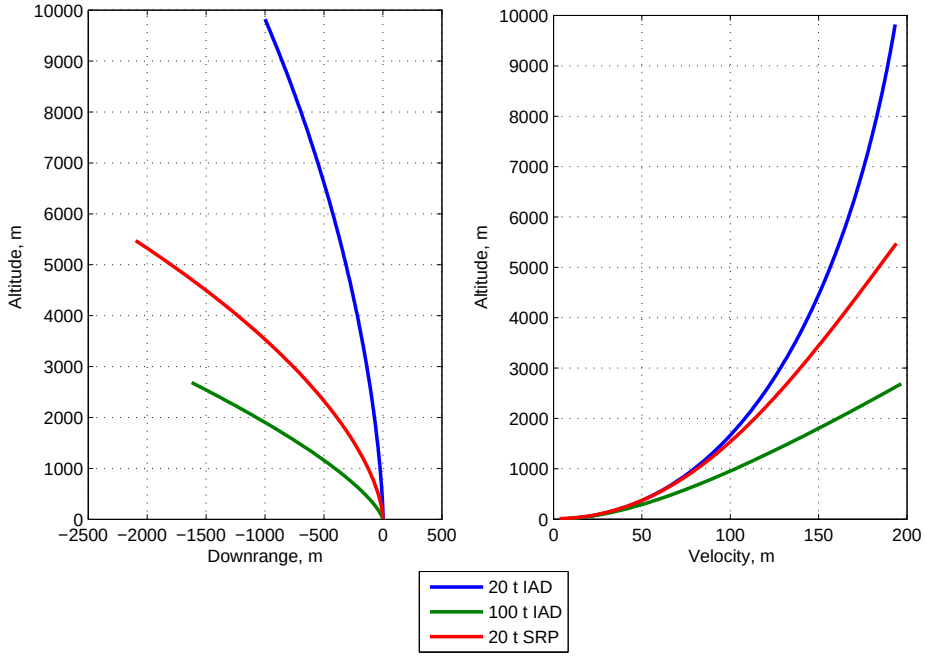

Figure 3: Nominal propulsive descent trajectories for each of the examined cases (20 t IAD, 100 t IAD, and 20 t SRP).

Each trajectory begins at the nominal PDI conditions specified in Table 2 ($t = 0$ s) with a landing site target identical to that of a constant thrust gravity turn. At the LPR time, $t = t_{\text{LPR}}$, the landing site is redesignated from the nominal trajectory landing site to an alternate landing site. The distribution of landing sites is dependent on the case. As seen in Fig. 4, landing sites located 5 and 10 km from the nominal are considered for the 20 t entry system depending on the supersonic deceleration technology. For the 100 t entry system, the analysis is focused on landing sites at 1.25 and 2.5 km from the nominal landing site. It should be noted that in initial studies, a 10 km radius was considered for each landing site, with the radii subsequently limited to feasible divert distances in order to increase the resolution of the results. For all vehicles, the landing sites are varied by 45 degree increments. The difference in distances from the nominal landing site is a result of the different trajectories for each scenario. For instance, the 20 t vehicle with a supersonic IAD begins PDI at approximately 10 km altitude, while the same vehicle using SRP initiates PDI at approximately 5 km altitude. Accordingly, the feasible divert distance diminishes as the altitude decreases.

Similarly, the LPR times (t_{LPR}) from PDI are also varied by case: times of 0, 20, and 40 s are used for the 20 t entry mass (IAD and SRP) while times of 0, 10, 20 s are used for the 100 t entry mass. The termination of the trajectory occurs when the altitude of the vehicle is less than 10 m. Should this termination condition occur within 200 m of the redesignated landing site, the landing is considered successful and used in the following analysis. These three time intervals were chosen to represent early, nominal, and late diverts. The early divert represents an idealized scenario where no additional processing time is needed once PDI occurs. In this scenario, the decision-maker (automated or human) is diverting to a pre-selected site, implying that no sensor anomalies occurred and the landing scenario meets expectations. A nominal divert is representative of a sensor scan and landing site selection ($\sim$5 s for automation, $\sim$12-

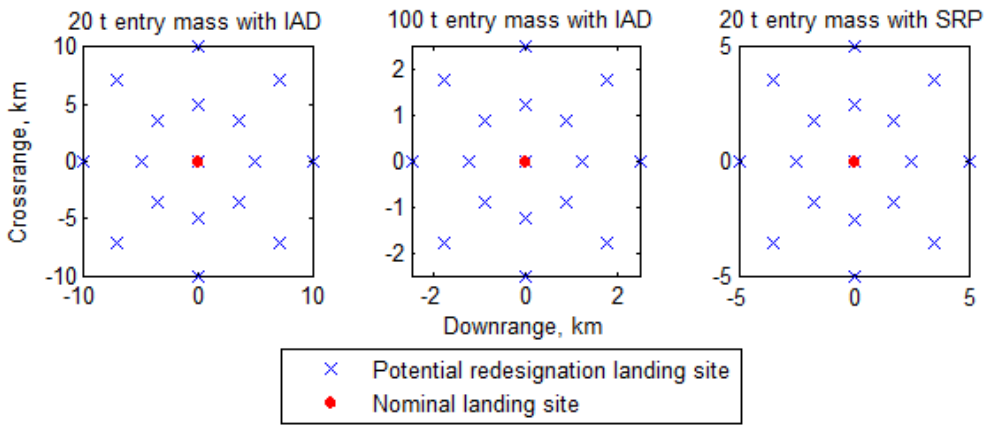

Figure 4: Landing Site Pattern.

28s for human[14]). Finally, a late divert represents the case where the crew or the automation may have had difficulty identifying the landing terrain, a likely outcome if the actual terrain greatly differs from expectations. In this analysis, a late divert occurs at least halfway into the nominal trajectory. These times are summarized in Table 3.

Table 3: Summary of the divert times for the different cases.

Divert Case	**Description**	t_{LPR} **for 20 t Entry Mass with IAD**	t_{LPR} **for 100 t Entry Mass with IAD**	t_{LPR} **for 20 t Entry Mass with SRP**
Early	*A priori* knowledge of divert	0 s	0 s	0 s
Nominal	Sensor data acquisition after PDI	20 s	10 s	20 s
Late	Difficulty in identifying terrain	40 s	20 s	40 s

D. Vehicle Sizing

The vehicle payload capability is calculated based on first-order models described in Steinfeldt *et al.*[7] These models are principally historical regressions for the subsystems against physical parameters seen during the descent and landing. The relation used to size the payload is shown in Eq. (1), where a 15% margin is applied to the dry mass.

$$\begin{aligned} m_{\text{payload}} = \quad & m_{\text{entry}} - 1.15(m_{\text{Structure}} + m_{\text{Heatshield}} + m_{\text{Backshell}} + m_{\text{RCS System}} + m_{\text{Decelerator}} \\ & + m_{\text{Propulsion System}}) - m_{\text{RCS Propellant}} - m_{\text{Propellant}} - m_{\text{Propellant Margin}} \end{aligned} \tag{1}$$

For the deterministic analysis, it is assumed that the trajectory prior to PDI is constant for each case considered. Therefore, the subsystems are sized based on those physical characteristics. The structure ($m_{\text{Structure}}$), the heatshield ($m_{\text{Heatshield}}$), the backshell ($m_{\text{Backshell}}$), the decelerator mass (IAD or SRP) ($m_{\text{Decelerator}}$), the reaction control system (RCS) ($m_{\text{RCS System}}$), and the reaction control system propellant ($m_{\text{RCS Propellant}}$) are assumed to be fixed and equal to the nominal cases' values. The terminal descent propellant ($m_{\text{Propellant}}$), propulsion system mass ($m_{\text{Propulsion System}}$), and the associated propellant margin ($m_{\text{Propellant Margin}}$) are the only parameters influencing payload mass that vary. The probabilistic analysis accounts for varied system mass at PDI based on the dispersions listed in Table 4.

The propulsion system is sized based on the relations shown in Eq. (2), where it is assumed that a LOx/CH_4 engine with an oxidizer-to-fuel ratio of 3.5 is used. When using these relations, a 10% margin is applied to the propellant

mass.

$$\begin{aligned} m_{\text{Propulsion System}} &= m_{\text{Engine}} + m_{\text{Tank}} \\ m_{\text{Engine}} &= 0.00144 T_{\text{max}} + 49.6 \\ m_{\text{Tank}} &= m_{\text{Tank-Fuel}} + m_{\text{Tank-Oxidizer}} \\ m_{\text{Tank-Fuel}} &= 0.2027 m_{\text{Fuel}} \\ m_{\text{Tank-Oxidizer}} &= 0.0750 m_{\text{Oxidizer}} \end{aligned} \tag{2}$$

The engine is sized according to the maximum thrust along the trajectory, which is limited to three times the initial weight of the vehicle relative to Earth. Note that this value is similar to using a Space Shuttle Main Engine for the 20 t entry mass and is consistent with prior studies.[11,12] Adjusting this value for the maximum thrust-to-weight will dramatically alter the results of this study, particularly the reach of the vehicle. Once the masses of all of the major subsystem components have been calculated accordingly, they are subtracted from the entry mass. This implies that the payload mass is not explicitly sized, rather, it is the remainder of this subtraction.

E. Vehicle and Trajectory Dispersions

The two IAD landing systems are also probabilistically analyzed. Dispersions are applied to the vehicle aerodynamics, characteristics, and state in order to obtain the mean and standard deviation of the payload mass for each potential redesignated landing site. These dispersions are shown in Table 4. The state dispersions are the result of propagating an entry interface state covariance matrix from the Mars Science Laboratory project with the appropriate atmospheric and aerodynamic uncertainties to the PDI condition. As seen in Fig. 5, this propagation results in an initial position of the vehicle varying horizontally from the nominal position to a maximum of 8 km away. The altitude uncertainty is to be within 1.5 km of the nominal PDI condition specified. These dispersions are similar to previous work such as those in Steinfeldt[1] and Grant.[4]

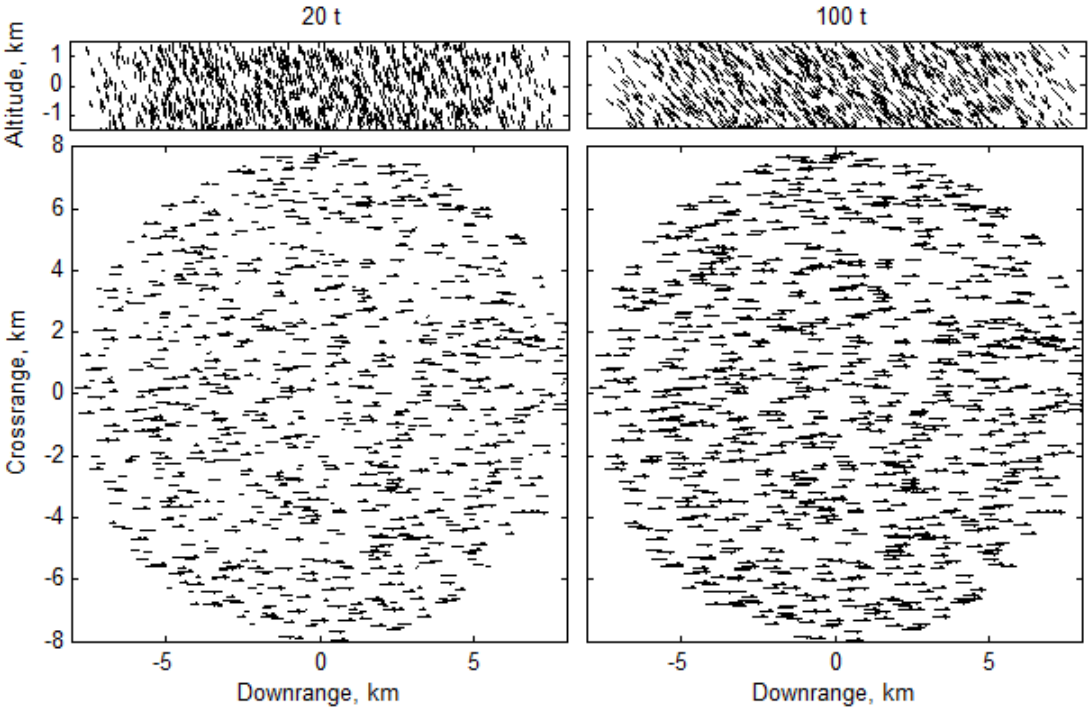

Figure 5: Initial position and velocity dispersions for the 20 t and 100 t entry masses.

Table 4: Vehicle and trajectory dispersions.

Parameter	Nominal	Distribution	Deviation (3σ or min/max)
Initial Mass	m_0	Gaussian	$0.03m_0$
Horizontal Distance from Nominal	0 km	Uniform	$\pm$ 8 km
Altitude Distance from Nominal	0 km	Uniform	$\pm$ 1.5 km
Initial Velocity	v_0	Gaussian	$0.03v_0$
Initial Flight Path Angle	γ_0	Uniform	$\pm 10\%$
Initial Azimuth angle	0°	Uniform	$\pm 5^\circ$
Density (10 km $< h <$ 30 km)	Profile	Uniform	$\pm 30\%$
Density ($h <$ 10 km)	Profile	Uniform	$\pm 15\%$
C_D multiplier ($0.8 < M < 5$)	1	Gaussian	0.10
C_D multiplier ($M < 0.8$)	1	Gaussian	0.05
Terminal Descent Engine I_{SP}	350 s	Uniform	$\pm 0.67\%$

III. Results

A. Deterministic Analysis

The results presented in this section describe the change in payload mass with respect to both the redesignated landing site location and when the divert is made. The changes in payload capability are a consequence of the system sizing discussed in Section D. Each redesignated site is referenced to the nominal landing site (*i.e.*, the site at the origin of each plot) by evaluating the difference in payload mass - negative values indicate less payload carried to that specific landing target.

Figure 6 illustrates the payload mass penalty associated with a 20 t entry vehicle at each of the three divert times. For the early divert and nominal divert, the vehicle is capable of reaching all divert sites within 10 km of the baseline point (0,0). However, the amount of payload that can be landed on the surface is dependent on the range and the redesignation time. For the early divert case (*i.e.*, $t_{LPR} = 0$ s), 10 km diverts incur a penalty over 1,000 kg, while a LPR time of 20 s to the same divert distance reduces the payload of the vehicle by $\sim$1,400 kg (payload mass fraction, PMF = 0.07). The PMF is defined as $m_{\text{payload}}/m_{\text{entry}}$, where entry mass is 20 t or 100 t. As the redesignation becomes later, the slight payload bias downrange is exacerbated. That is, the payload penalty is lower for downrange diverts compared to reverse downrange. When the landing site is redesignated 40 s into the trajectory, the payload penalty is more severe, with a $\sim$2,100 kg (PMF = 0.11) loss in potential payload capacity if the vehicle is required to divert 10 km. It should also be noted that diverting 40 s into the trajectory leads to some reverse downrange landing sites not being achievable. This limitation of options is due to the limited thrust-to-weight capability of the vehicle with the implementation of the guidance algorithm, which is unable to provide suitable deceleration to achieve the landing site. This case is not true of further diverts in the reverse downrange direction due to the loft solution that is the optimal unconstrained trajectory for these sites.

As the vehicle becomes more massive the trajectory is shifted lower in the atmosphere, resulting in LPR occurring at a lower altitude. This lower altitude results in the divert flexibility being greatly reduced. As seen in Fig. 7, while the vehicle can divert up to 1.25 km downrange, reaching sites behind the nominal requires more propellant and a higher thrust. For a 1.25 km divert in the positive downrange direction, the payload mass penalty is $\sim$100 kg (PMF = 0.001), while the same divert in the negative downrange direction has a payload mass penalty of $\sim$900 kg (PMF = 0.009). These numbers, while small, also represent one-eighth the divert distance capability of a 20 t entry vehicle. Landing site options decrease the longer it takes to make a decision. Redesignating 10 s from PDI reduces the reverse downrange capability to 1.25 km, and at 20 s, landing sites are only achievable within 1.25 km downrange of the baseline site and 2.5 km in crossrange. The additional crossrange capability is a result of the additional timeline due to a "helix" type guidance solution. This "helix" trajectory increases the timeline and requires less thrust than a comparable divert solely along the downrange direction.

These results suggest the importance of making rapid landing decisions to reduce fuel consumption and retain LPR divert range capability. While it may be argued that humans are incapable of selecting a landing site this quickly, studies focused on decision-making during LPR illustrate that flight experience and type of automated assistance

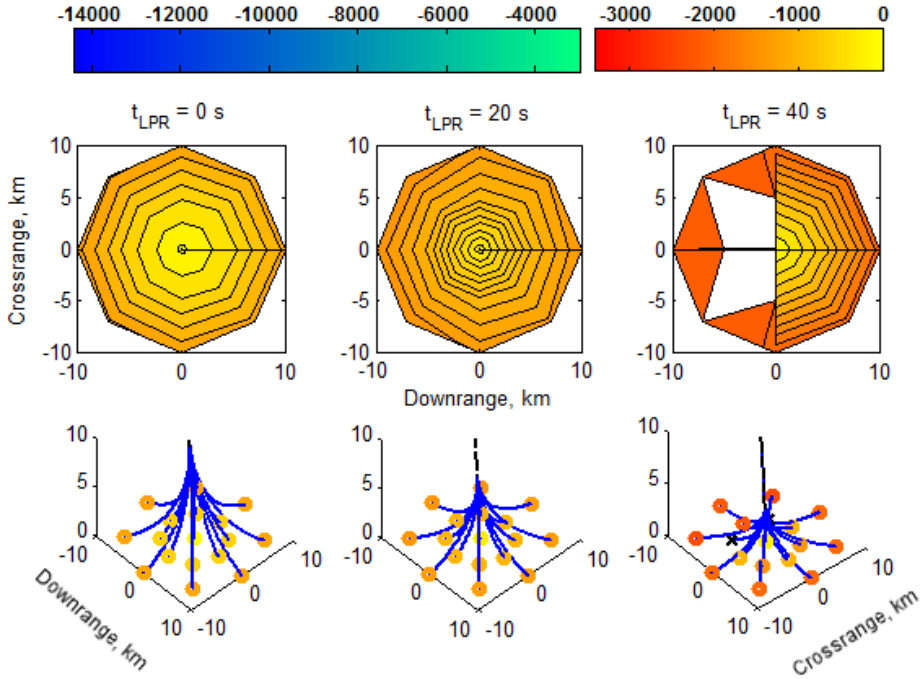

Figure 6: 20 t entry mass deterministic analysis, for t_{LPR} = 0, 20, 40 s.

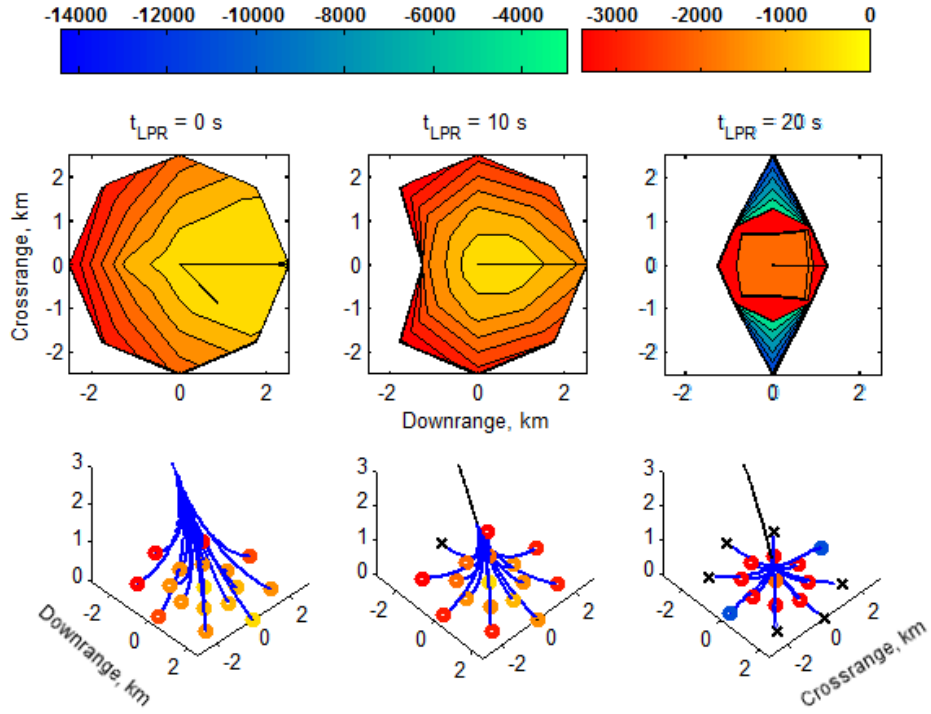

Figure 7: 100 t entry mass deterministic analysis, for t_{LPR} = 0, 10, 20 s.

can greatly reduce the LPR decision-making time. A recent experiment involving helicopter pilots (average flight experience of 1129 h) using one representative LPR automation interface illustrated that pilots can perform the task between 5-15 s.[15] In contrast, the same task involving fixed-wing pilots (average flight experience of 216 h) with another LPR automation interface produced higher performance times, between 12-28 s.[16]

B. Probabilistic Analysis

A Monte Carlo analysis was used to examine the sensitivity to vehicle and trajectory dispersions for both the 20 t and the 100 t entry mass cases. Two different analyses were conducted: one which examined the mean payload mass and its variance for each of the potential redesignated sites; and one which examined the landing ellipse characteristics. These analyses were again conducted for three divert times: early ($t_{LPR} = 0$ s), nominal ($t_{LPR} = 20$, 10 s), and late ($t_{LPR} = 40$, 20 s) for the 20 t and 100 t entry masses, respectively.

Figures 8 - 13 show a relative depiction of the mean payload variation for each site as well as its standard deviation. For each landing site, a pair of "bubbles" is plotted. The area of the inner bubble represents the average payload mass deviation from the nominal across all successful Monte Carlo runs for the site, while the area of the outer bubble represents the 1σ payload deviation from the nominal for the site. Thus, the gap between the two bubbles indicates the magnitude of the standard deviation. The bubbles plotted at each redesignated landing site are first normalized with respect to the nominal landing site, then scaled linearly relative to each other to increase the visibility of the plot's trends. Therefore, a bubble with twice the area of another bubble does not indicate a payload mass deviation from the nominal twice as large. Instead, the average and standard deviation of payload mass deviation from the nominal is reported for both the largest and smallest bubbles, and all other bubbles scale linearly between those two values. Additionally, each landing site is labeled with the percent of Monte Carlo cases that landed successfully.

Figures 14-19 illustrate the landing ellipses for the various landing sites as well as the percentage of successful landings for each site. Landing ellipses at 1 and 3σ were plotted based on sites that were within 200 m of their designated landing sites.

1. 20 t Entry Mass

The probabilistic analysis on the 20 t entry mass illustrates similar characteristics to the deterministic analysis. For early diverts (t_{LPR} = 0s), diverts as far as 10 km are possible, while late diverts limit the distance of the divert to 5 km with a high probability of success. In addition to reducing the likelihood of a successful landing, delaying the divert from 0 s to 40 s increases the 1σ payload deviation from $\sim$800 kg to $\sim$1,700 kg (PMFs from 0.04 to 0.09) for the minimum (nominal) payload deviation site and from $\sim$1,800 kg to $\sim$21,000 kg (PMFs from 0.09 to 1.05) for the maximum payload deviation site. For late diverts this is significant as the nominal payload mass is only 9.2 t for the vehicle. Therefore the vehicle is not capable of reaching these distances. The 3σ landing ellipses along the downrange direction are circular, with all attempts landing very closely to the designated site. Crossrange diverts skew the ellipse, with an increase in eccentricity as the distance of the divert increases.

2. 100 t Entry Mass

The probabilistic analysis on the 100 t entry mass, however, shows the challenges of landing such a sizable payload on the Martian surface. Early and nominal diverts are possible to up to 2.5 km while ensuring that approximately 75% of the cases land successfully. For late diverts this distance must be limited to 1.25 km in order to maintain a similar probability of success. This is similar to the results of the deterministic analysis for this case. For late diverts (*i.e.*, t_{LPR} = 20 s), the maximum 1σ payload deviation is more than three times that of early diverts ($\sim$46,000 kg when t_{LPR} = 20 s as compared to $\sim$14,000 kg when t_{LPR} = 0 s) while the minimum only doubles ($\sim$12,000 kg when t_{LPR} = 0 s versus $\sim$24,000 kg when t_{LPR} = 20 s). Similar landing ellipse characteristics to the 20 t entry mass are exhibited, with downrange diverts being skewed along that direction, crossrange diverts being skewed crossrange, and off diagonal diverts being skewed in the direction of the divert.

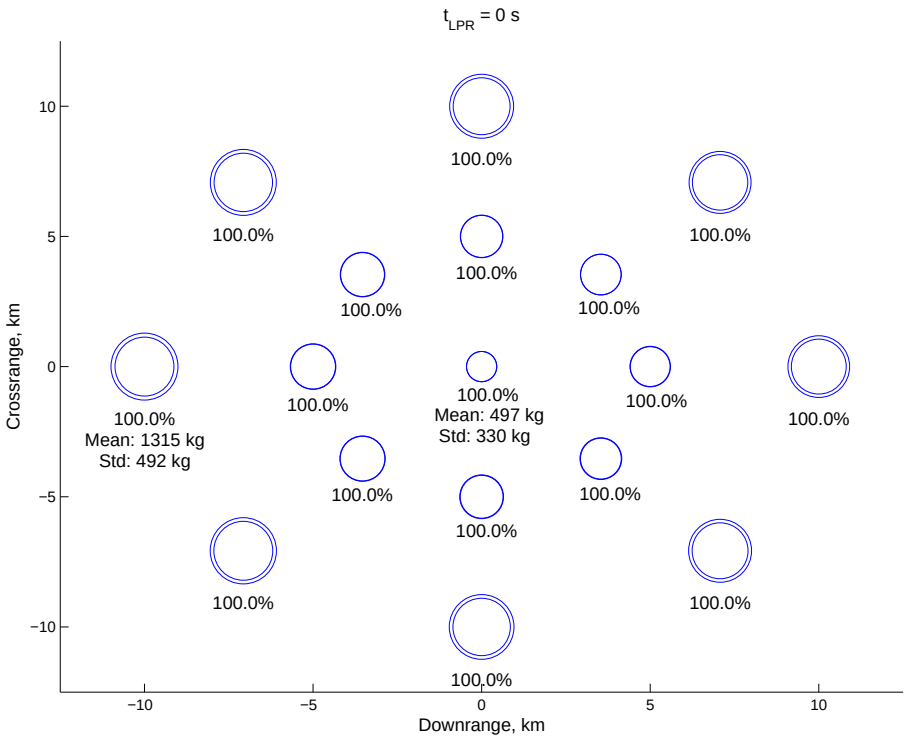

Figure 8: Payload mass mean deviation and standard deviation for the 20 t entry mass for $t_{LPR} = 0$ s.

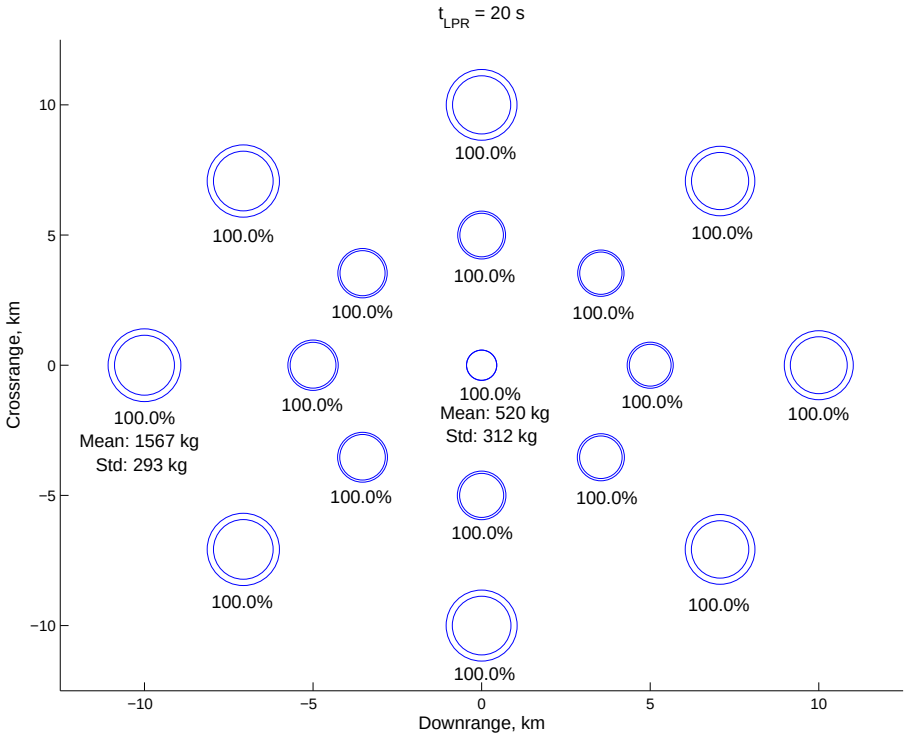

Figure 9: Payload mass mean deviation and standard deviation for the 20 t entry mass for $t_{LPR} = 20$ s.

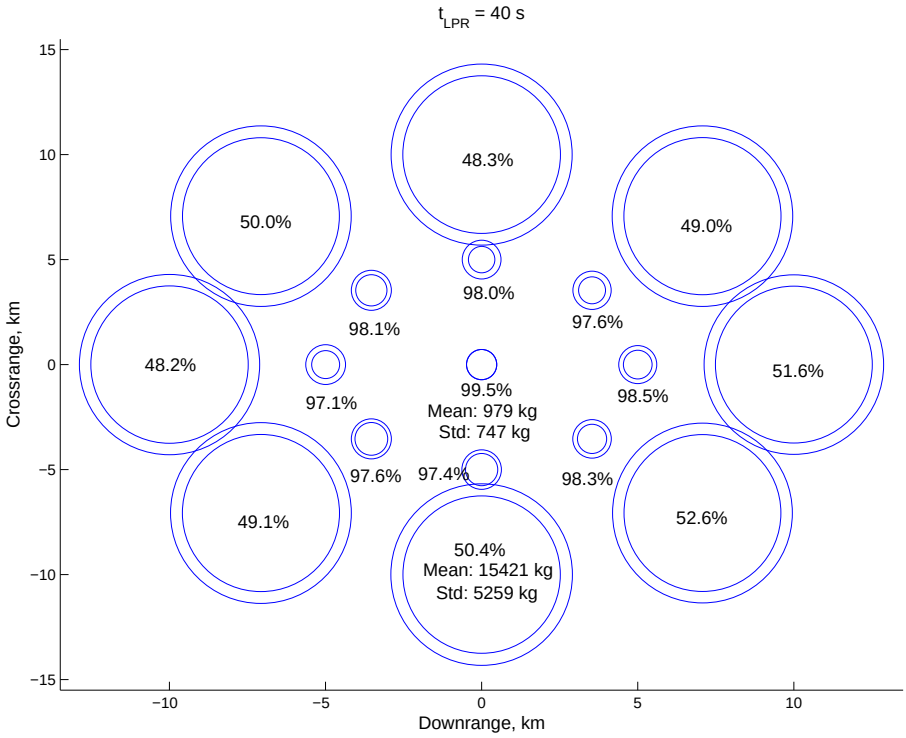

Figure 10: Payload mass mean deviation and standard deviation for the 20 t entry mass for $t_{LPR} = 40$ s.

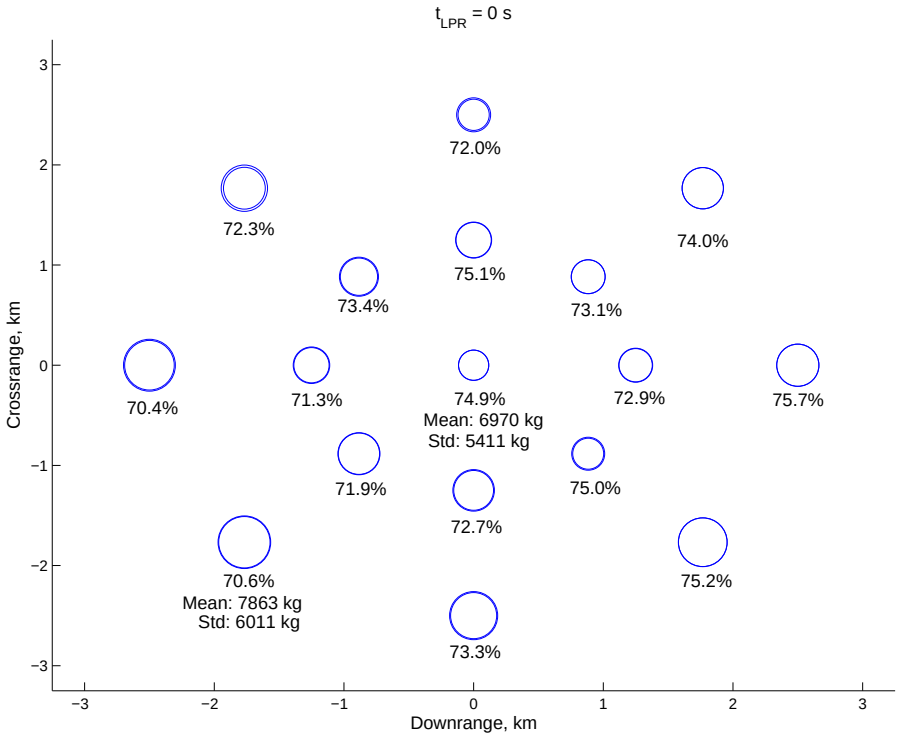

Figure 11: Payload mass mean deviation and standard deviation for the 100 t entry mass for $t_{LPR} = 0$ s.

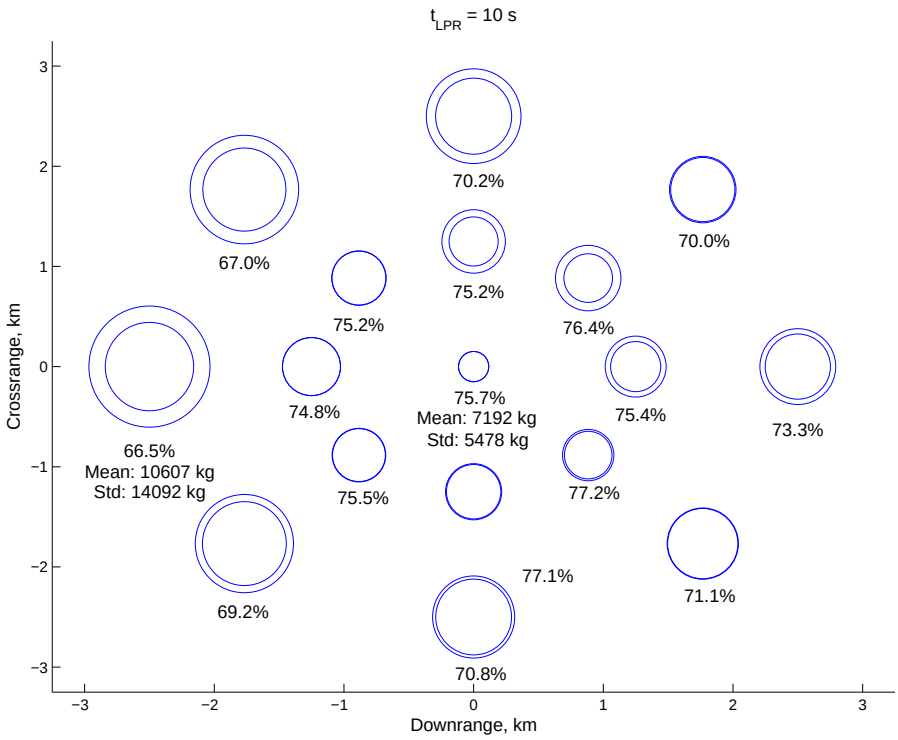

Figure 12: Payload mass mean deviation and standard deviation for the 100 t entry mass for $t_{LPR} = 10$ s.

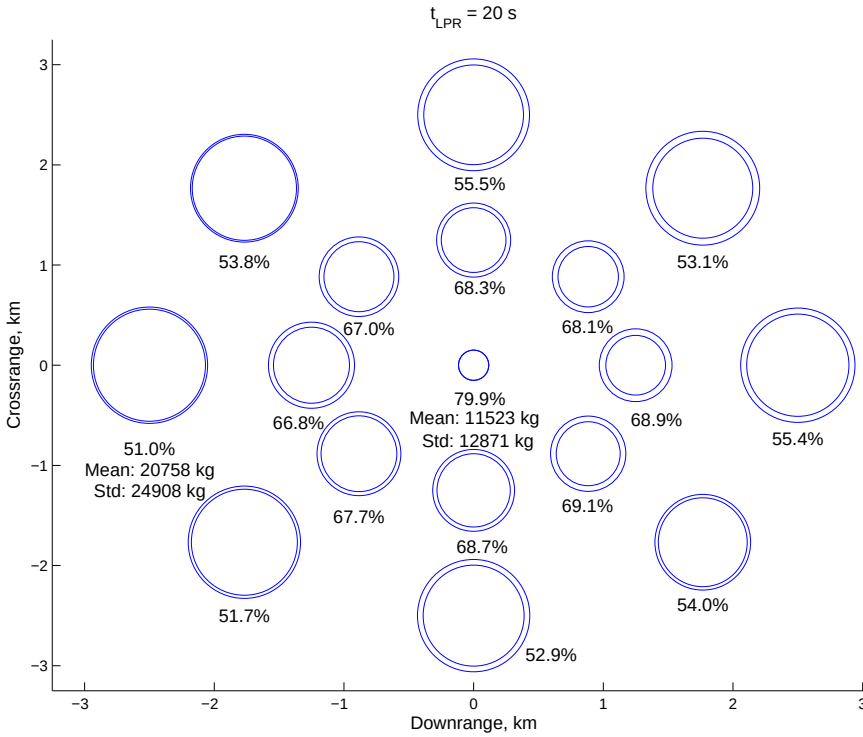

Figure 13: Payload mass mean deviation and standard deviation for the 100 t entry mass for $t_{LPR} = 20$ s.

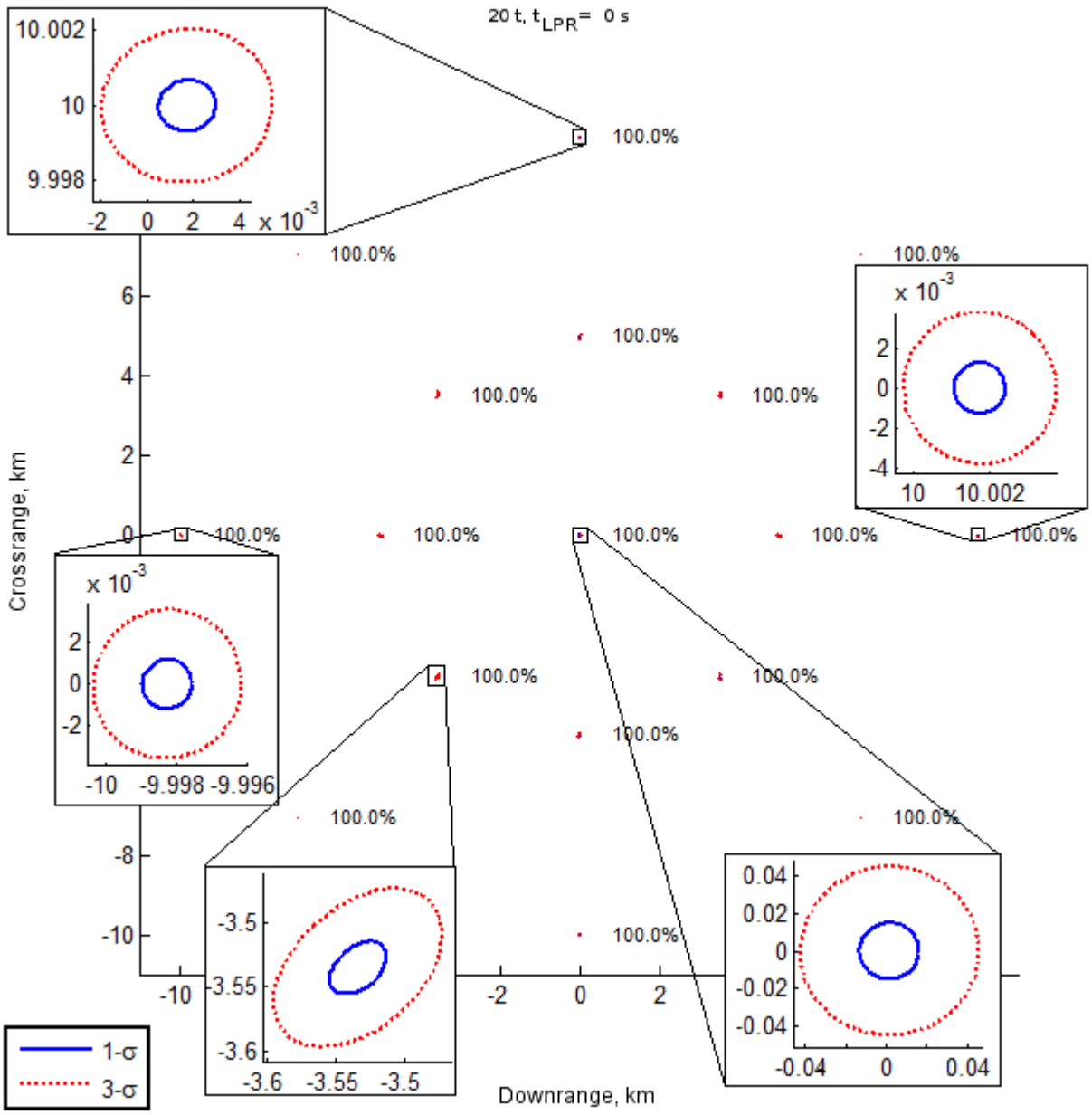

Figure 14: 20 t entry mass landing ellipses for $t_{\mathrm{LPR}} = 0$ s.

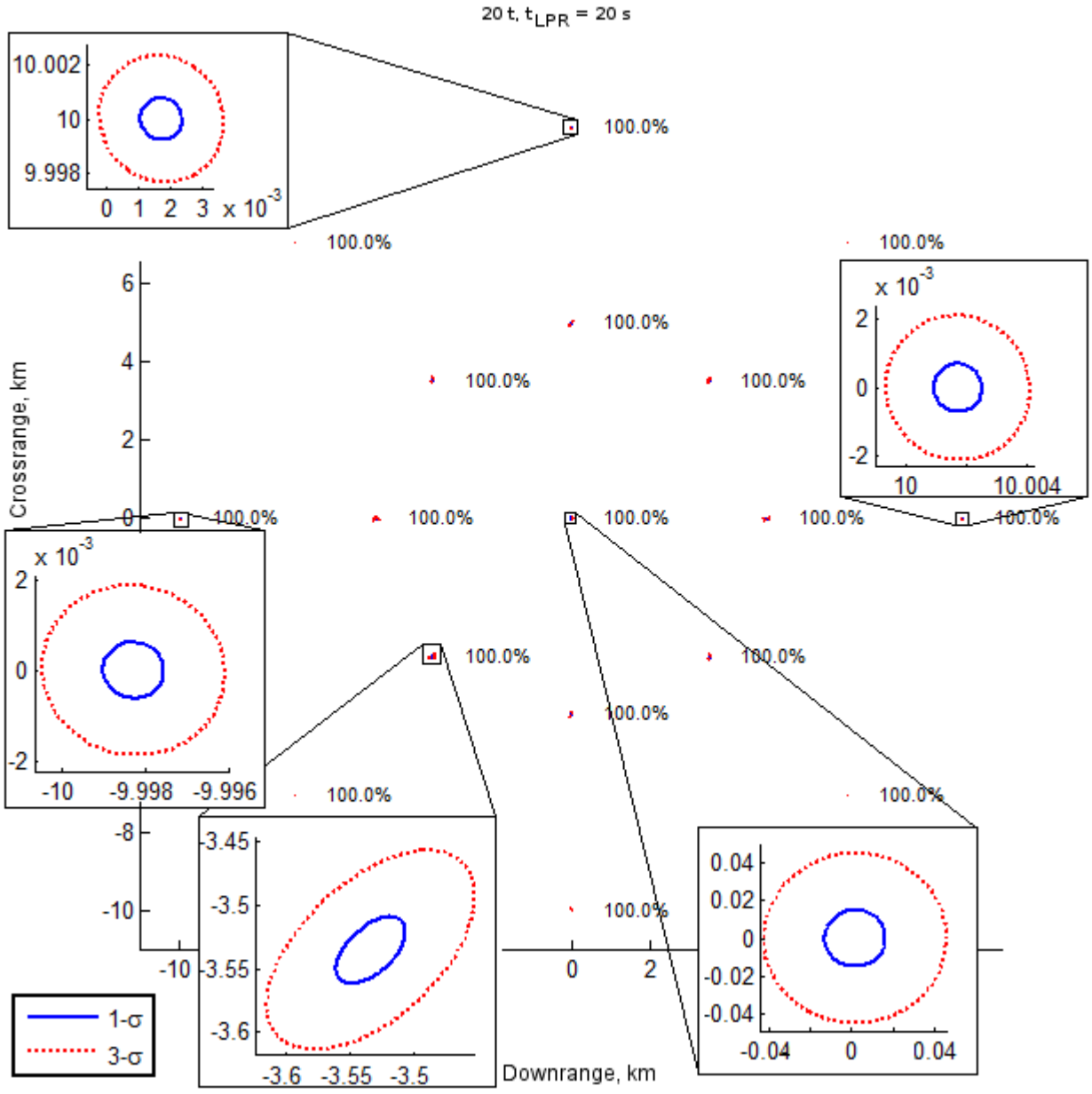

Figure 15: 20 t entry mass landing ellipses for t_{LPR} = 20 s.

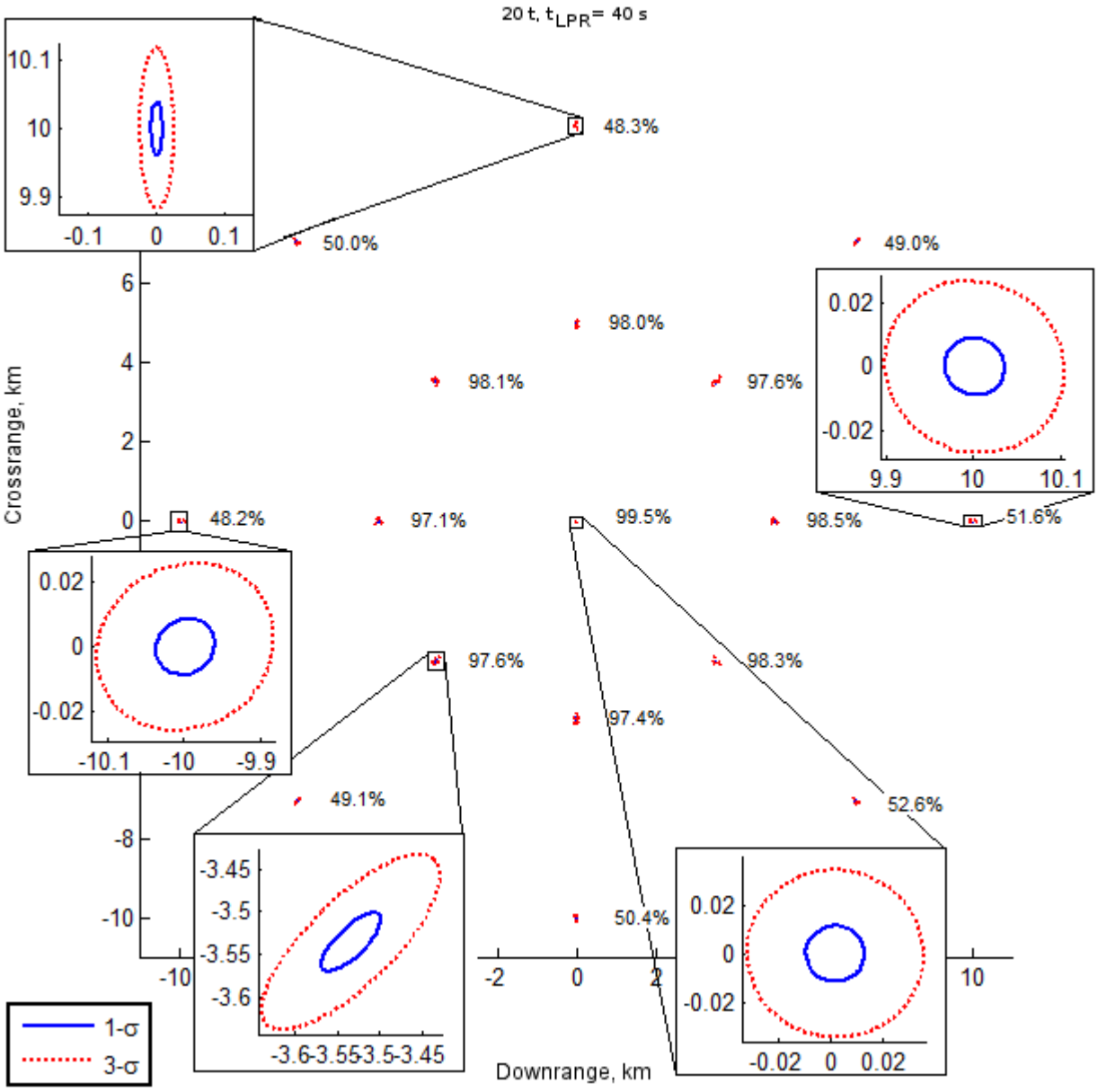

Figure 16: 20 t entry mass landing ellipses for $t_{\mathrm{LPR}} = 40$ s.

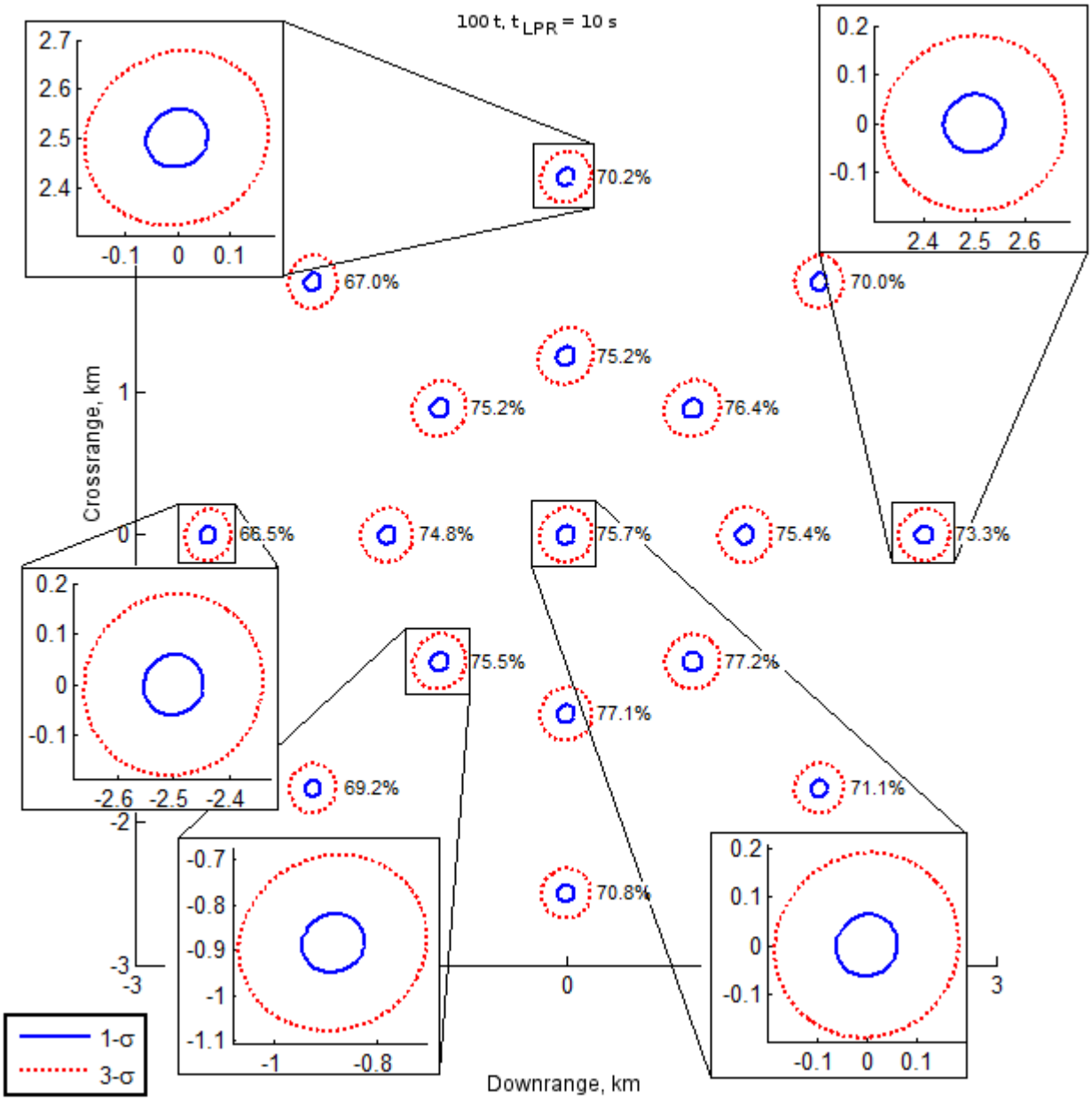

Figure 17: 100 t entry mass landing ellipses for $t_{\mathrm{LPR}} = 0$ s.

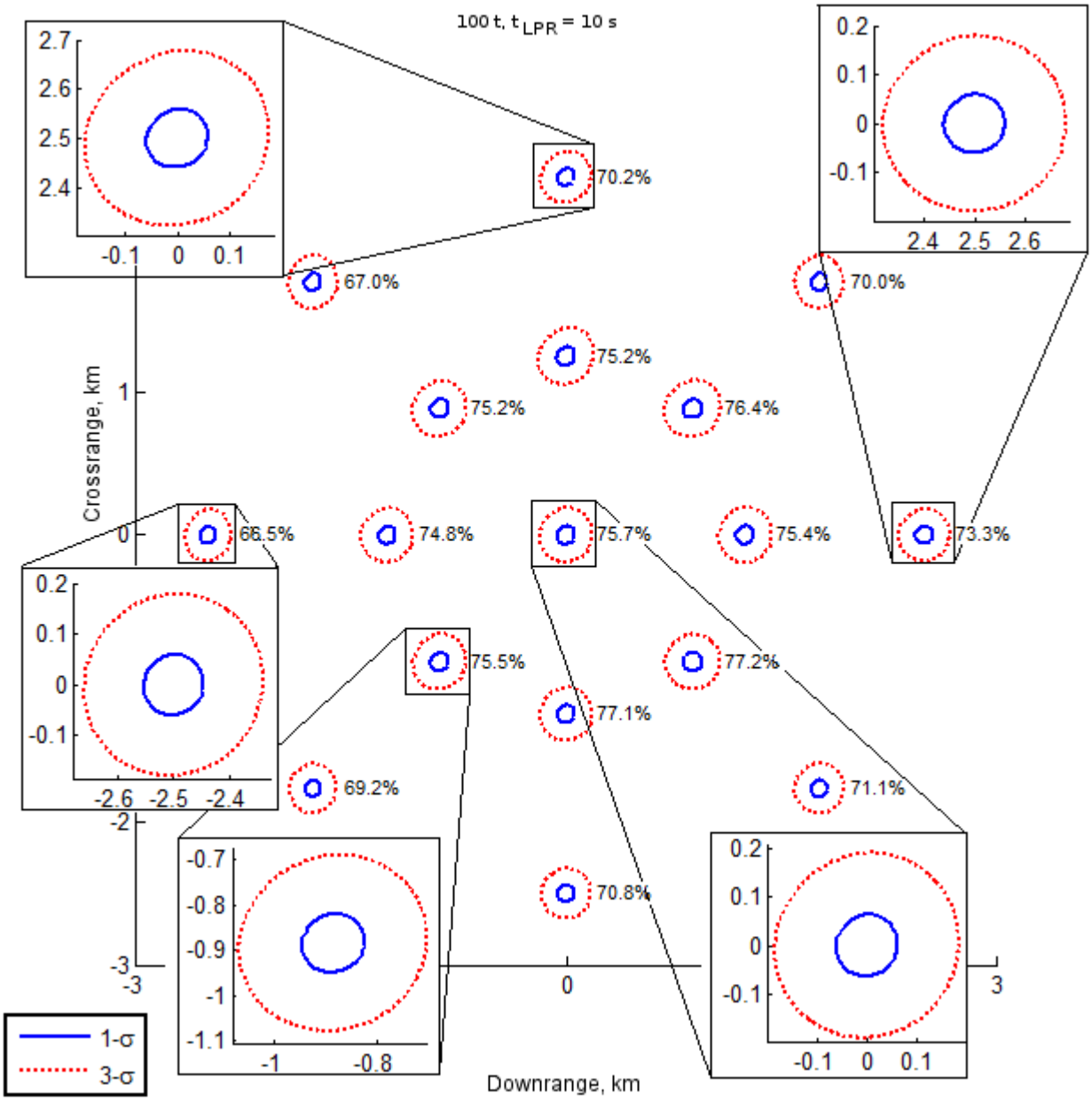

Figure 18: 100 t entry mass landing ellipses for t_{LPR} = 10 s.

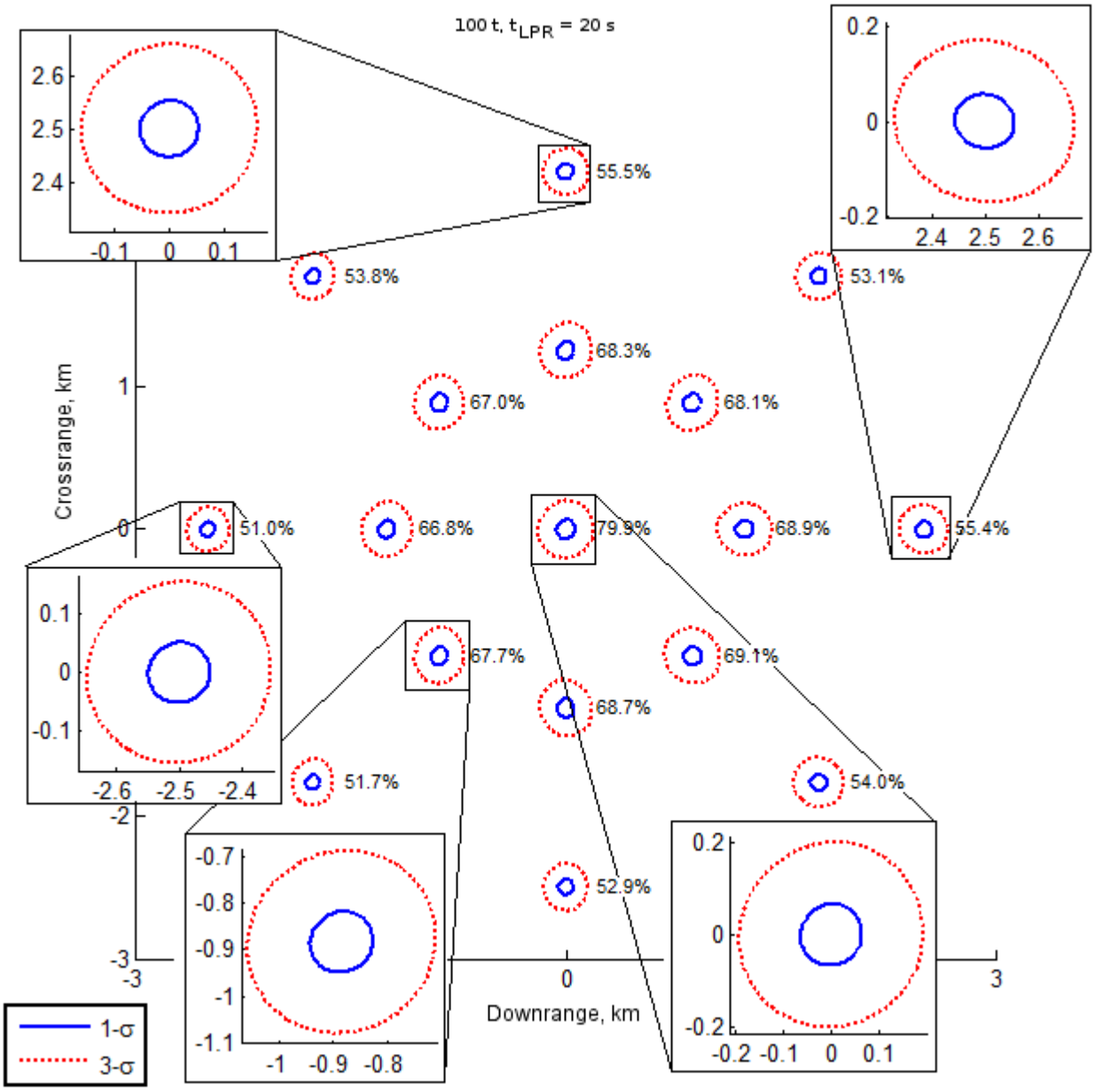

Figure 19: 100 t entry mass landing ellipses for t_{LPR} = 20 s.

C. Supersonic Deceleration Technology Comparison

The performance of a 20 t entry vehicle with SRP was also considered in this study. The SRP system is used later in the trajectory, with LPR occurring around 5 km altitude instead of 10 km. Fig. 20 illustrates the payload mass change depending on the time and divert site. This case follows similar trends to Figs. 6 and 7: downrange capability is greater than reverse downrange and later decisions result in increased payload mass penalty. The range capability is less in the SRP case than IAD due to the trajectory profile associated with this supersonic deceleration technology. The initial altitude is approximately 5 km less than the equivalent IAD case. Due to the additional acceleration required to achieve targets, there is approximately a 500 kg payload penalty relative to the IAD. However, the shallower flight-path angle allows additional timeline for all of the reverse downrange cases to be achievable. While not investigated in this work,

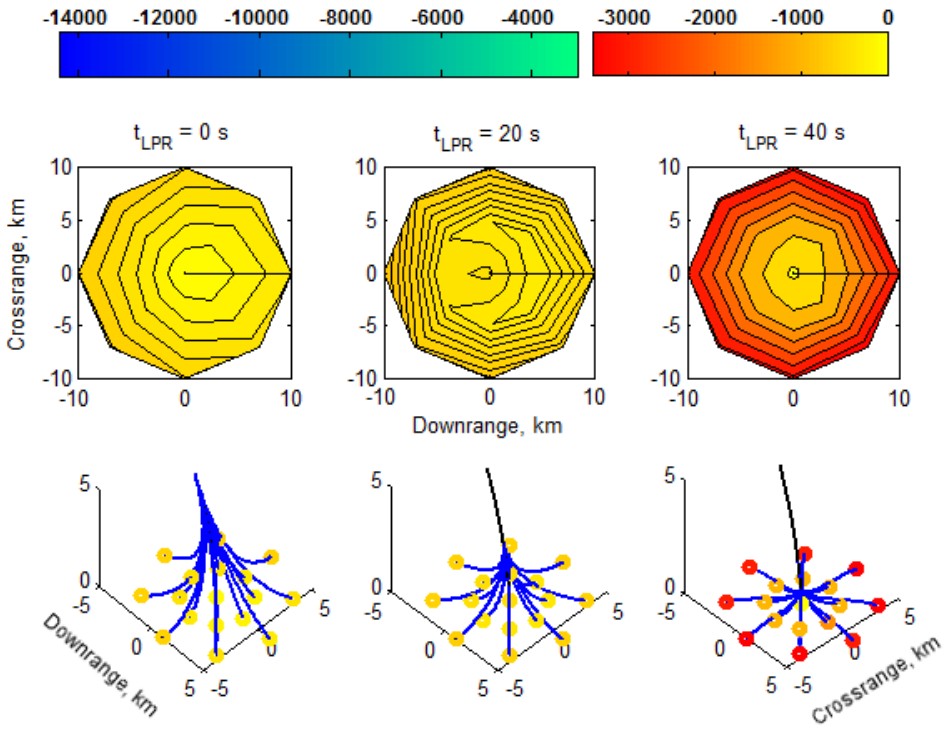

Figure 20: 20 t entry mass with an SRP deterministic analysis, for t_{LPR} = 0, 20, 40 s.

it should be mentioned that during the supersonic phase with a throttleable engine and appropriate sensing technology, it may be possible to redesignate while using SRP in the supersonic regime. This would have apparent mass benefits relative to the subsonic redesignation times chosen in this study. The apparent benefit of the supersonic redesignation would be similar to that of comparing the 20 t and 100 t entry mass cases, with a larger reachable set of landing sites as well as a diminished payload penalty.

IV. Discussion

The results from this preliminary analysis present the impact of landing point redesignation on system design via the change in payload mass. Consequently, from this analysis one can also determine the divert reach capability. Many of the observed results are related to ballistic coefficient effectsmore massive vehicles decelerate lower in the atmosphere and are unlikely to be capable of diverting far from their landing sites. This effect limits the divert distance and for feasible diverts increases the propellant required. In addition to these ballistic coefficient effects, the fact that landing point redesignation is occurring as the vehicle is traversing (as opposed to a fixed altitude, hovering position), the location of the landing site with respect to the nominal site is critical. Landing downrange of the intended site is easier than diverting reverse downrange. In some instances, the divert range capability is equal, but a greater propellant penalty is incurred. In other instances, the reverse downrange divert capability is reduced. The propellant usage, along

with a maximum thrust, is used to size the system and evaluate consequences in an appreciable systems-level value: a loss of payload mass. Second, the payload mass penalty for some diverts can be severe, up to 14,000 kg. Allowing for divert capability (time and distance) becomes a delicate tradeoff with payload mass for mission designers.

The modification of the guidance algorithm to have limited thrust-to-weight capability had a significant influence in the distance of the divert. Increasing this value beyond the 3.0 (relative to Earth) considered in this study would certainly increase the distance of divert achievable by the entry system. In addition, the guidance algorithm has no knowledge of this constraint, except through state feedback. Should this constraint be directly incorporated in the formulation of the guidance law, the trajectories would be shaped differently and the number of achievable landing sites would likely be increased at the expense of propellant mass. Also, the authors acknowledge that given the state of pinpoint landing technology, landing within hundreds of meters of an intended site may be possible with appropriate navigation technology.[1] The current study defined a successful landing as within 200 m to be near the limit of what is achievable by state-of-the-art guidance and navigation systems for Mars entry systems.[1] If the proximity aspect of the successful landing definition is indeed increased, the vehicle would be capable of diverting farther than that indicated in this study.

This analysis does not provide any insight on who or what will determine when and how far to divert, or the outcome of the decision-making. As seen in other studies such as those performed by Chua *et al.*, several combinations of function allocation between an onboard human, a remote human, and an automatic landing system are possible.[14,16] Due to the communication delay between Mars and Earth, this divert decision cannot be performed real-time by a remote human. It is likely the decision will be performed by a combination of human and automation interaction. Current analyses cite 12-28 s decision time at a high level of automation.[16] These decision times are achievable for less massive entry vehicles with PMF penalties for LPR capability of $\sim$0.10 for 10 km diverts, for more massive vehicles (on the order of 100 t entry mass) this severely limits the divert capability of the vehicle and may cause unacceptably large PMFs of $\sim$0.45 for the ability to perform LPR.

V. Conclusions

The results from this preliminary analysis present the impact of landing point redesignation on system design in the change in payload mass as well as reachable divert distances. It was seen that the maximum change in PMF for the feasible early diverts was similar between the two entry systems using supersonic IADs (PMF penalties of $\sim$0.07 and $\sim$0.08, for the 20 t mass and 100 t mass, respectively) while later diverts impacted the payload capability of the vehicles significantly (PMF penalties between $\sim$0.21 and $\sim$0.78). Early diverts for the 20 t case were able to reach over 10 km from the nominal landing site with a payload mass penalty of $\sim$1,300 kg (PMF = 0.07), while late diverts limited the divert distance to half of this distance (5 km) with a payload mass penalty of $\sim$15,000 kg (PMF = 0.18). For the 100 t case, vehicles were able to reach 2.5 km downrange with a payload mass penalty of $\sim$8,000 kg (PMF = 0.03) for an early divert while late diverts limited the range to less than 1.25 km with nearly 15,000 kg of a payload mass penalty (PMF = 0.14). Finally, using SRP increased the PMF by $\sim$0.03 as compared to an IAD. All of these effects are a result of the staging trajectory. More massive vehicles decelerate lower in the atmosphere; similarly, delaying the divert also causes the vehicle to decelerate lower in the atmosphere. This not only limits the divert distance, but also requires more control effort (*i.e.*, propellant) to achieve a soft landing. These effects would be mitigated by increasing the thrust-to-weight ratio allowed by the trajectory; however, deceleration g-limits and propulsion technology limits provide a practical upper bound for this value.

Acknowledgments

The authors thank the National Aeronautics and Space Administration (NASA) who funded the work discussed here as part of the Reentry Aerothermodynamics Virtual Institute of the Constellation University Institutes Project (CUIP). In addition, the authors thank their colleagues within the Space Systems Design Laboratory at Georgia Tech who have provided valuable insight into this work, in particular, Juan G. Cruz-Ayoroa and Cole D. Kazemba.

References

[1] Steinfeldt, B. A., Grant, M. J., Braun, R. D., and Barton, G. H., "Guidance, Navigation, and Control System Performance Trades for Mars Pinpoint Landing," *Journal of Spacecraft and Rockets*, Vol. 47, No. 1, January-February 2010, pp. 188–198.

[2] Klump, A. R., "Apollo Lunar-Descent Guidance," Tech. Rep. R-695, MIT Charles Stark Draper Laboratory, Cambridge, Massachusetts, June 1971.

[3]Sostaric, R. R., "Powered Descent Trajectory Guidance and Some Considerations for Human Lunar Landing," *2008 IEEE Aerospace Conference Paper Number 1316*, March 2008.

[4]Grant, M. J., Steinfeldt, B. A., Braun, R. D., and Barton, G. H., "Smart Divert: A New Entry, Descent and Landing Architecture," *Journal of Spacecraft and Rockets*, Vol. 47, No. 3, May-June 2010, pp. 385–393.

[5]Bonfiglio, E., Adams, D., Craig, L., et al., "Landing Site Dispersion Analysis and Statistical Assessment for the Mars Phoenix Lander," *AIAA Paper 2008–7348*, Aug. 2008.

[6]Adams, D., "Phoenix Mars Scout Landing Risk Assessment," *2008 IEEE Aerospace Conference Paper Number 1316*, March 2008.

[7]Steinfeldt, B. A., Theisinger, J. E., Korzun, A. M., Clark, I. G., and Braun, R. D., "High Mass Mars Entry, Descent and Landing Architecture Assessment," *AIAA Paper 2009–6684*, Pasadena, CA, Sept. 2009.

[8]Clark, I. M., Hutchings, A. L., Tanner, C. L., and Braun, R. D., "Supersonic Inflatable Aerodynamic Decelerators for Use on Future Robotic Missions to Mars," *Journal of Spacecraft and Rockets*, Vol. 46, No. 2, March-April 2009, pp. 340–352.

[9]Korzun, A. M. and Braun, R. D., "Performance Characterization of Supersonic Retropropulsion for High-Mass Mars Entry Systems," *Journal of Spacecraft and Rockets*, Vol. 47, No. 5, September-October 2010, pp. 836–848.

[10]Drake, B. G., "Human Exploration of Mars Design Reference Architecture 5.0," Tech. Rep. SP-2009-566, NASA, 2009.

[11]Cianciolo, A. M. D. et al., "Entry, Descent and Landing Systems Analysis Study: Phase 1 Report," Tech. Rep. TM-2010-216720, NASA, 2010.

[12]Andrews, D. G., Cannon, J. H., Lund, E. A., and Watry, K. E., "High Mass Mars Entry System Architecture Design and Technology," Tech. Rep. CR-2009-NNL08AA35C, NASA, 2009.

[13]D'Souza, C. N., "An Optimal Guidance Law for Planetary Landing," *AIAA Paper 1997–3709*, New Orleans, LA, Aug. 1997.

[14]Chua, Z. K., Braun, R. D., and Feigh, K. M., "Analysis of Human-System Interaction For Landing Point Redesignation," Masters ae 8900 project, Georgia Institute of Technology, 2009.

[15]Chua, Z. K. and Feigh, K. M., "Pilot Decision-Making during Lunar Landing Point Designation," *Cognition, Technology, and Work*, 2011, To be submitted.

[16]Chua, Z. K., Feigh, K. M., and Braun, R. D., "Examination of Human Performance during Lunar Landing," *2010 IEEE Aerospace Conference*, No. IEEEAC 1150, Big Sky, MT, 2010.